Effects of Electromagnetic Stimulation and Rapamycin on Morphology and Autophagy of In-vitro Cultured Spiral Ganglion Neurons

Radišić, Dubravko

Master's thesis / Diplomski rad

2024

Degree Grantor / Ustanova koja je dodijelila akademski / stručni stupanj: **University of Split, Faculty of Science / Sveučilište u Splitu, Prirodoslovno-matematički fakultet**

Permanent link / Trajna poveznica: https://urn.nsk.hr/urn:nbn:hr:166:148062

University of Split
Faculty of Science

Effects of Electromagnetic Stimulation and Rapamycin on Morphology and Autophagy of in-vitro cultured Spiral Ganglion Neurons

Master thesis

Dubravko Radišić

Split, September 2024

Temeljna dokumentacijska kartica

Sveučilište u Splitu
Prirodoslovno-matematički fakultet
Odjel za fiziku
Ruđera Boškovića 33, 21000 Split, Hrvatska

Diplomski rad

Utjecaj elektromagnetske stimulacije i rapamicina na morfologiju i autofagiju *in-vitro* uzgojenih kultura neurona spiralnog ganglija

Dubravko Radišić

Sveučilišni diplomski studij Fizika, smjer Biofizika

Sažetak:
Neuroni spiralnog ganglija (NSG) su primarni auditorni neuroni odgovorni za prijenos auditornog signala iz osjetnih stanica s dlačicama do kohlearne jezgre u mozgu. Njihova degeneracija, uz oštećenje osjetnih stanica s dlačicama, jedan je od glavnih uzroka zamjedbenog (senzoneuralnog) gubitka sluha (SNHL). Efikasnost najuspješnijeg uređaja medicinske bionike, kohlearnog implantata (umjetne pužnice), ovisi o broju i funkcionalnom stanju NSG. U ovome radu promotrili smo utjecaj primjene elektromagnetskog polja i indukcije autofagije preko primjene rapamicina, esencijalnog staničnog procesa odgovornog za održavanje homeostaze i zdravlja stanica, kao potencijalnu kombiniranu metodu promoviranja većeg rasta i zdravlja neonatalnih NSG-ova. Rezultati su pokazali da EMF stimulacija utječe na autofagiju, te da kombinacija rapamicina i EMF stimulacije može postići značajno veći rast NSG-ova. Ovaj efekt, kao i utjecaj na morfološke karakteristike i stanično zdravlje, varirao je s različitim koncentracijama rapamicina. Ovaj rad pokazuje da se modulacija autofagijske aktivnosti u kombinaciji sa drugim metodama može koristiti kao potencijalna terapeutska strategija za pobolšanje efikasnosti umjetne pužnice.

Ključne riječi: Neuroni spiralnog ganglija, autofagija, elektromagnetsko polje, rapamicin, morfologija neurona

Rad sadrži: 49 stranica, 11 slika, 27 tablica, 58 literaturnih navoda. Izvornik je na engleskom jeziku

Mentor: izv. prof. dr. sc. Damir Kovačić

Ocjenjivači: izv. prof. dr. sc. Damir Kovačić
doc. dr. sc. Ivana Weber
doc. dr. sc. Mija Marinković

Rad prihvaćen: 26. 9. 2024.

Rad je pohranjen u knjižnici Prirodoslovno-matematičkog fakulteta, Sveučilišta u Splitu.

Basic documentation card

University of Split
Faculty of Science
Department of Physics
Ruđera Boškovića 33, 21000 Split, Croatia

Master thesis

Effects of Electromagnetic Stimulation and Rapamycin on Morphology and Autophagy of In-vitro Cultured Spiral Ganglion Neurons

Dubravko Radišič

Graduate university study programme Physics, specialisation in Biophysics

Abstract:
Spiral ganglion neurons (SGN) transmit auditory signals from sensory-receptive hair cells to the cochlear nucleus in the brain. Damage to hair cells typically leads to degeneration of SGN and represents one of the leading causes of sensorineural hearing loss (SNHL) worldwide. The effectiveness of the most successful auditory prosthetic, the cochlear implant, in treating SNHL depends on the number and health of preserved SGNs. In this study, we assessed whether autophagy induction via rapamycin, a crucial cellular process responsible for maintaining cellular homeostasis and health, can be combined with a pulsed electromagnetic field (EMF) stimulation to strengthen the growth and health of neonatal SGNs, cultured *in-vitro*. The results showed that EMF stimulation plays a role in autophagy and that combining rapamycin and EMF stimulation strengthens the SGN outgrowth significantly. This effect and the impact on morphological characteristics and cellular health varied sensitively with different concentrations of rapamycin. This study demonstrates that modulation of autophagic activity, in combination with other methods, may be utilized as a potential therapeutic strategy to enhance the efficacy of cochlear implants.

Keywords: Spiral ganglion neurons, autophagy, electromagnetic field, rapamycin, neuron maturation

Thesis consists of: 49 pages, 11 figures, 27 tables, 58 references. Original language: English

Supervisor: Associate Professor Damir Kovačić, Ph.D.

Reviewers: Associate Professor Damir Kovačić, Ph.D.
Assistant Professor Ivana Weber, Ph.D.
Assistant Professor Mija Marinković, Ph.D.

Thesis accepted: September 26, 2024

The thesis is deposited in the library of the Faculty of Science, University of Split.

Firstly, I would like to thank my mentor, Assoc. Prof. Damir Kovačić for guidance and advice during my Bachelor and Master studies. It was a pleasure to work alongside him, and I am truly grateful for the opportunities he provided. I would also like to thank all the other members of Kovacic Lab.

Next, I would like to thank Ana Bedalov for scientific, practical, and life advice, as well as the opportunity to find my strengths during my stay at KARMENStudio. I would also like to thank all my current and former colleagues at KARMENStudio for the much-needed help in image analysis and for the many laughs and good times.

I would also like to thank Dr. Bastien Duckert, my supervisor and friend at imec v.z.w. (Leuven, Belgium) for all the patience and training. Furthermore, I would like to thank all the wonderful colleagues and friends there (LST and further) who made my stay in Belgium unforgettable (absolutely too many to name here). Likewise, I would like to thank Prof. Myles Mc Laughlin for the opportunity to stay at the Experimental Oto-rhino-laryngology group, KU Leuven. Although short, my lab visit helped me to further expand my practical knowledge and connected me with even more wonderful students and colleagues.

As for all of my professors and assistants at the Faculty of Science, University of Split, Department of Physics, I have nothing but kind words, as I am sure it is not always an easy job. I believe all of them still uphold the appropriate standard while still caring for the students. As for my colleagues and friends with whom I shared this journey, I thank you because, without your help, I am quite sure I would not have been here (The first year was rough). In all of you, I not only found friends, I found inspiration, and every one of you has taught me at least one thing.

I give a special thank you to all my friends, who can mostly be abbreviated by thanking all the previous and current members of my folklore group *KUD Ante Zaninović*. You have given me a home, many life lessons, love, and support, and you have all shaped my young and adult life. You will all always be with me. I'm not including names since I'm sure somebody would protest; those to whom it applies will know already.

And to the strongest woman I know, thank you, my mother, for everything. I would not be here if it weren't for your many sacrifices and continual support. I am proud to be called your son.

And to my father, I hope to live up to your words; you are my greatest inspiration.

Contents

1 Introduction

Biological cells are constantly exposed to stressors, from environmental changes to internal metabolic activities. To function optimally and, in extreme cases, to survive, they rely on a delicate balance of physiological and metabolic processes that regulate their internal environment, collectively known as cellular homeostasis. Maintaining homeostasis is critical for cell viability, as imbalances can lead to dysfunction, disease, or even cell death. Notably, the cell's ability to manage and dispose of damaged proteins, organelles, and other cellular components represents an essential aspect of the cellular life cycle. This dynamic process allows cells to adapt to changing conditions, prevent the toxic accumulation of dysfunctional components, and efficiently recycle essential nutrients. Among the mechanisms responsible for this is autophagy, an essential cellular process of waste and damaged cellular components recycling, which is responsible for maintaining cellular homeostasis. It is present in almost all types of cells and is especially important in maintaining cell health of post-mitotic cells. The process itself consists of several steps: encapsulation of cargo with the phagophore, formation of the autophagosome, autophagosome fusion with the lysosome, a membrane-bound cell organelle filled with digestive enzymes, and degradation of cargo and recycling (Fig. 1).

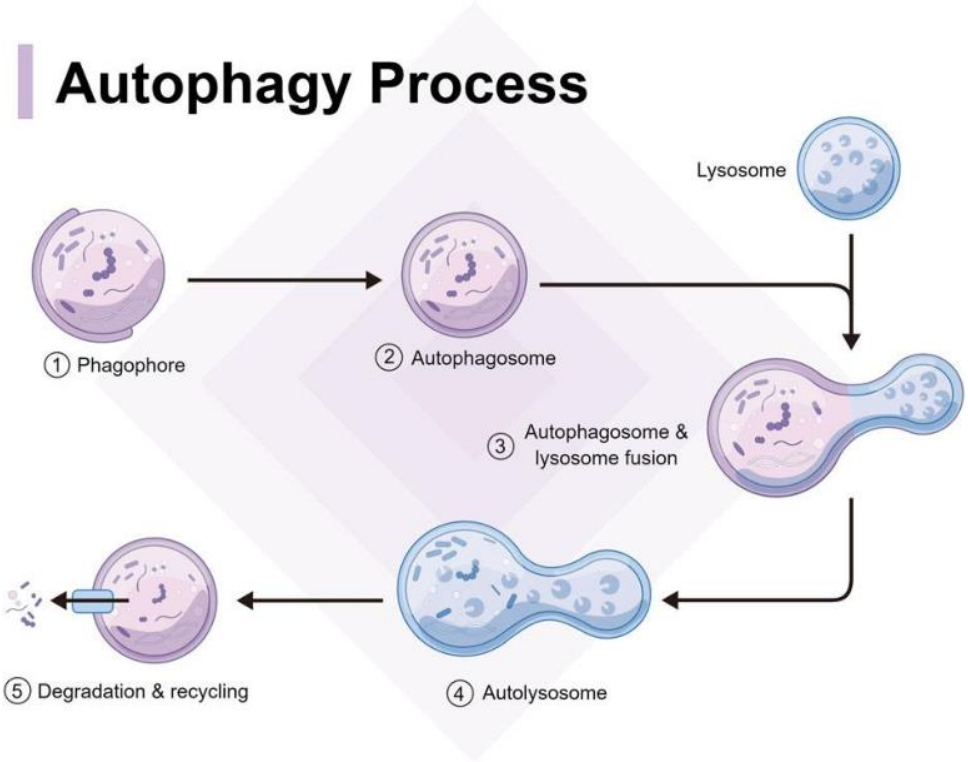

Figure 1. *A basic schematic depiction of the autophagy process. Taken from [1]*

There are several types of autophagy based on their selectivity and mechanisms. Most broadly, autophagy can be divided into macroautophagy, which is the typical process as defined in Fig.

1., where larger cell components such as protein aggregates or organelles are enveloped by a double-membrane autophagosome and then transported to the lysosome for degradation, microautophagy, where smaller structures like vesicles or soluble proteins enter the lysosome directly for degradation, and chaperone-mediated autophagy, where cargo is brought into the lysosome through specific active transport channels (Fig. 2.). There is also selective and non-selective autophagy, where non-selective degrades bulk cargo regardless of type, and selective can target specific molecules or organelles for e.g. mitophagy which is a selective type of autophagy which targets mitochondria.

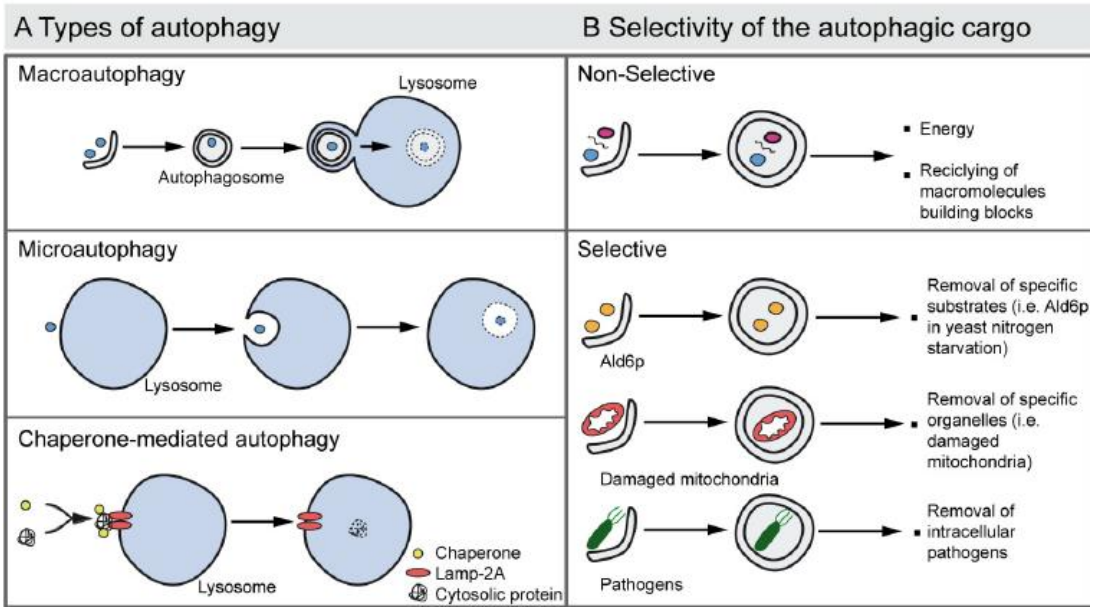

Figure 2. *Schematic depiction of general autophagy classification. Taken from [2]*

Macroautophagy, also known as bulk autophagy, is the most common autophagy type and is the most widely researched and analyzed in terms of its prevalence and relative ease of examination. Macroautophagic modulation as a therapeutic technique is widely recognized for its potential because it has a role in almost any type of cellular dysfunction and damage. However, many challenges stand in the way of utilizing this process effectively [4]. Issues are of practicality, autophagy induction specificity, and a lack of knowledge regarding the exact molecular mechanisms of its regulation, which is troublesome because, in excess, autophagy can induce autophagic cell death (Type II cell death), apoptosis (Type I cell death) and is linked with necrosis [3]. Therefore, autophagy modulation should be carefully implemented.

Autophagy plays an important role in sensorineural hearing loss (SNHL) [5]. World Health Organization (WHO) estimates that around 5% of the population is affected by some form of hearing loss, the leading type of which is SNHL [6]. In short, damage to inner and outer hair cells leads to degeneration of spiral ganglion neurons (SGN). Significant advances in hair cell

regeneration using stem cell and gene therapy have been made [5]. However, in the context of the cochlear implant, a widely applied neuro-prosthetic device that innervates spiral ganglion neurons (SGNs), now the survival, health, and guided growth of SGNs form a basis for restoring hearing ability. Since SGNs are non-mitotic, guiding their growth towards the electrode array and supporting their neuronal survival is essential. It is not clear whether the number of preserving and functioning SGNs influences hearing performance, as contradictory findings have been reported [7, 8]. Thus, many studies are now focused on reversing the process of degeneration, guiding growth, promoting stronger differentiation, or even inducing neurogenesis. [9-15]. In the context of autophagy, the most relevant approach to improving cochlear implants seems to be to ameliorate the effects of autophagy induction. Autophagy-inducing methods have been shown to reduce oxidative stress and remove the accumulation of waste proteins in ear hair cells, SGNs, and dorsal root ganglion (DRG) neurons in various stress environments; autophagy induction effects on near homeostatic SGNs remain unexplored [13, 16].

1.1 Spiral ganglion neurons and the cochlea

The cochlea is an inner-ear structure responsible for transforming the mechanical signal of sound to an appropriate electrical signal in the form of changes of trans-membrane potentials in the sensory cells, which can stimulate the auditory nerve. The spiral ganglion is a collection of cell bodies of the auditory nerve fibers residing in the central axis of the cochlea (seen on the cross-section image in Fig 3. The spiral ganglion innervates the sensory cells in the organ of Corti (Fig 4.) and transfers the signal toward the brain where the sound is being perceived. Specifically, spiral ganglion neurons (SGNs) are synaptically connected with inner and outer auditory hair cells (IHC, OHC), which act as mechanoreceptors. The spiral ganglion consists of two types of auditory neurons: Type I SGNs and Type II SGNs. Type I SGNs comprise around 95% of neurons in the spiral ganglion and are characterized by a smaller level of myelinization, bipolar morphology, and a larger cell body (cell soma). Whereas Type II SGNs make up only around 5% of the neuron population, their morphology is usually pseudo-monopolar, their soma is smaller, and it has various cytoskeletal and cytoplasmic differences (a lack of standard organelle, more microfilament etc.) [19].

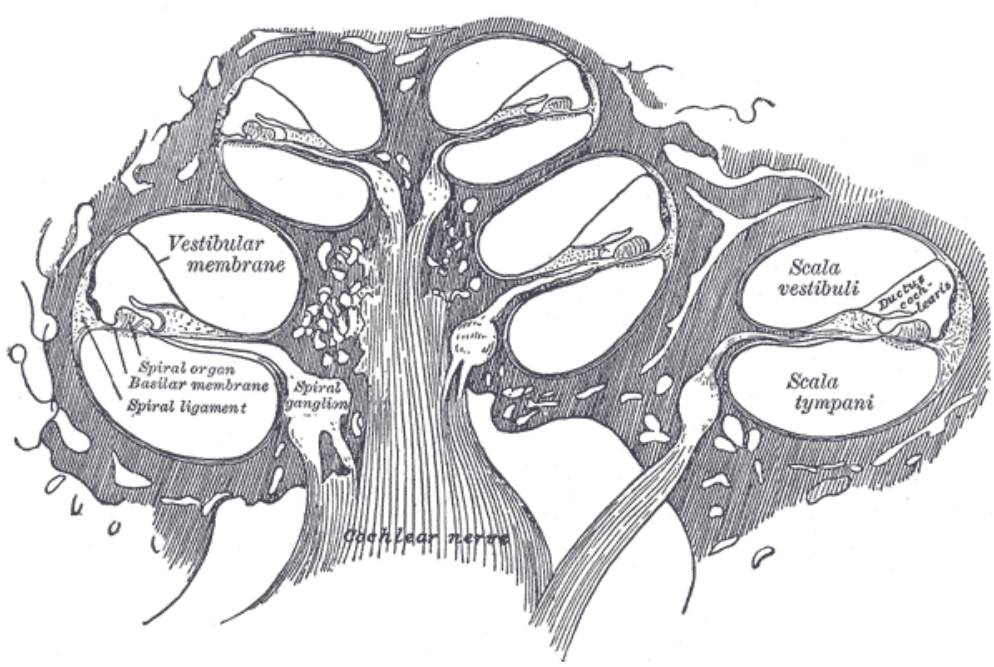

Figure 3. *A schematic cross-section of the cochlea. Taken from [17].*

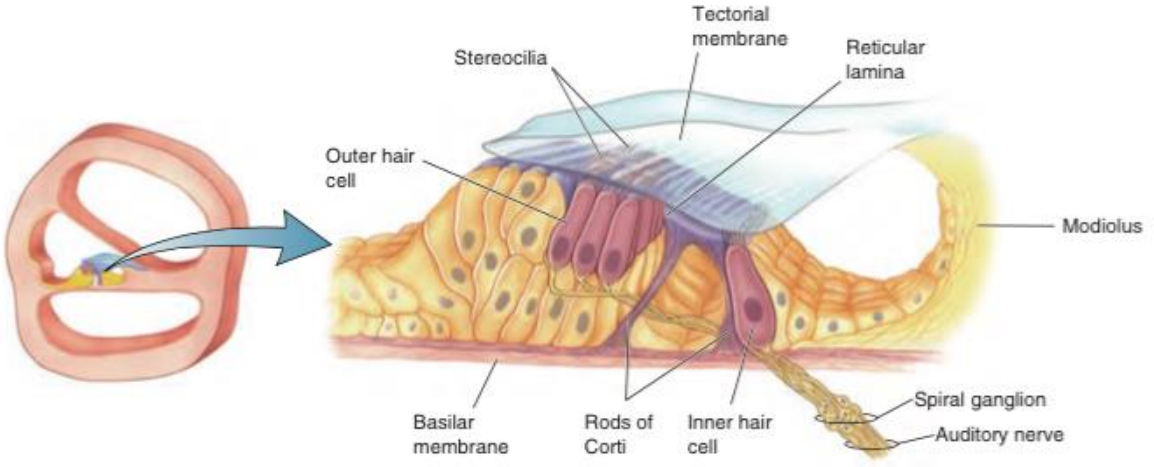

Figure 4. *An illustration of the organ of Corti. Taken from [18].*

1.2 Autophagy and mTOR

The mammalian target of rapamycin (mTOR) is a protein kinase, a specific type of enzyme responsible for controlling various cellular metabolic processes. The signaling pathway up-regulates and down-regulates autophagy and cell proliferation, also directly affecting the metabolism and is involved in cell death signaling pathways (apoptosis) [20, 21, 22].

Malfunctioned mTOR signaling is linked with various cancers and degenerative diseases, as over-activation of mTOR can cause protein aggregation and unhealthy cell growth [23]. Specifically, it is composed of two connected protein signaling complexes mTORC1 and mTORC2, which are interconnected but serve different functions. mTORC1 is activated by environmental cues such as starvation, energy consumption, as it is responsible for allocating resources for protein synthesis [21, 22]. Furthermore, it is one of the main autophagy-inhibiting complexes. Rapamycin inhibits mTORC1 function directly and is thus used as an autophagy activator. mTORC2, however, is regarded as not being affected by rapamycin. It has also been significantly researched, less than mTORC1. Its function is cell metabolism regulation, which is affected by growth factors and insulin. Both complexes have been linked with stress response, neurite regeneration and outgrowth [11,12].

1.3 Mechanisms of neurite guidance

Since the widespread and successful implementation of the cochlear implant, important studies have been made on guided axonal growth in SGNs [14, 15, 24, 25, 26, 27]. A particular aspect has been given to neuron regeneration and growth. As with any post-mitotic cells, methods of promoting regeneration, trans-differentiation and resistance to internal or external injury are of great interest because of their enormous therapeutic potential. For neurons, studies into neurogenesis or *in-vitro* on neonatal neurons have been particularly insightful as they have shed light on multiple pathways of neuronal guidance, health, and growth. The main mechanisms of axonal guidance are broadly divided into three categories: chemotaxis, in which neurotrophic factors and other growth factors are used as targeted markers for directional growth; electrotaxis, where electromagnetic stimulation of varying pulse lengths, amplitudes, and shapes are applied to the SGNs [29, 30, 31, 32], and mechanotaxis, in which mechanical and micro-topographical cues are specifically designed and fabricated on appropriate materials [14, 15, 25, 33]. Combining these mechanisms has also been shown to additionally promote neurite length and directionality [34, 35]. These discoveries led to various in-vivo therapies currently being tested; further *in-vitro* and *in-vivo* research is still necessary to address complex signaling cascades, specificity, and toxicity. As a construct placed in the cochlea's neuronal environment, the cochlear implant is at the forefront to benefit from this type of research.

1.4 Electrotaxis and SGNs

The use of electromagnetic fields for axonal guidance and regeneration has been mainly observed and researched in spinal cord and peripheral nerve injury, and promising results have been shown [36, 37, 38]. Surprisingly, there seems to be a shortage of research into electrotaxis outside this context. In the case of examining the effect of electromagnetic stimulation on SGNs, there seems to be very few publications [29, 39]. The significant complication of research on this topic is the sensitive nature of the experiments, where results with the same exposure parameters can have significantly different results depending on the cell type, cellular

microenvironment, age of the examined cells. Considering this, more parallelized and standardized experiments are needed. However, since the cellular and intracellular mechanisms also need explanation, we focus on a more fundamental *in-vitro* approach to examine morphological and intracellular changes on SGNs stimulated with a pulsed electromagnetic field (EMF).

1.5 Electromagnetic field and Autophagy

With the rise of radio-frequency EMF (RF-EMF) use in modern appliances, bulk of the research has been made on the effects of most common exposure parameters on oxidative stress, autophagy, and survival of various cell lines [40, 41]. Particularly investigated were neurons as they are one of the theorized most sensitive cell lines to such stimulation. Furthermore, nerve tissue damage can be more severe in terms of limited therapeutic options [32, 38, 42]. The interplay of EMF stimulation and autophagy has yet to be fully understood. Currently, the main consensus is that EMF stimulation activates autophagy either through reactive oxygen species (ROS) recruitment, which causes intracellular damage, or through silencing of miR-30a autophagy inhibition and not through thermic effects [43]. Here, we examine ROS as the potential mechanism of autophagy induction during SGN growth, either through oxidative stress-induced damage or general ROS signaling.

1.6 Reactive oxygen species

Reactive oxygen species are characterized as highly reactive byproducts of cellular metabolism, which in abundance can damage lipid, protein and DNA structures [44]. They are involved in various pathological conditions such as aging, cancer, and neurodegenerative disease. Besides this effect, ROS have been linked with an incredible amount of intercellular signaling pathways, which put redox homeostasis at the forefront of understanding cellular response to drugs and disease [45]. Specifically, ROS signaling was linked with, among others, transcription factor NF-κB (nuclear factor kappa-light-chain-enhancer of activated B cells) signaling, mitogen-activated protein kinase (MAPK) signaling, and phosphoinositide-3-kinase (PI3K)-Akt pathway [46]. Most of these pathways are strongly linked with mTOR as modulators of autophagic activity [47]. Due to these pathways' sensitivity, complexity, and interconnectivity, the disturbance of intracellular redox homeostasis as a therapeutic target should be carefully attempted.

1.7 A link with neurogenesis

Besides the involvement of autophagy in many homeostatic processes and complex intracellular interactions, it has also been significantly linked with embryonic development [48]. Multiple studies have shown the involvement of autophagy in cell differentiation and maturation, where autophagy-deficient animal models were shown to have significant developmental and psychological disorders [23, 49]. Moreover, autophagy and type II

autophagic cell death have been implicated in neurogenesis, spine, synaptic pruning, and synaptic plasticity [50, 51]. The mechanism of electrotaxis for neuron migration has been mostly observed in vivo during neurogenesis [30], where endogenic small electric gradients guide neurons to their destination; also, neuron regeneration via electric field stimulation-induced differentiation was linked with autophagy pathways [38]. Since this process has also been observed in the embryonic development of the cochlea and SGNs [51, 52], autophagy has been proposed to be the main driving force of electrical field guidance and as a potential target for promoting nerve regeneration, migration, and stem cell differentiation. Recently, autophagy induction via rapamycin was also shown to promote hair cell differentiation in neonatal mice inner ear organoids [53].

1.8 mTORC2 and SGN morphology

One of the most successful applications of axonal guidance is using microtopographical cues for directed neurite outgrowth and promoting health and more differentiation to neurons. Separately, various studies have shown a beneficial effect on neuron health and even on SGNs [14, 15, 33, 35, 54]. One study in particular sought to investigate the mechanotransductive signaling of dorsal root ganglion (DRG) neurons and found out that its investigated targets in 1D cultures, where neurons were cultured in a tube-like construct allowed to grow only in one dimension, along microtopographical cues of increased outgrowth, mTORC2 was the most significantly up-regulated [54]. General increased mTOR activity was observed, and mTORC2 co-localized at growth cones at the regenerating front. Although previously regarded as not being directly involved with autophagy and unaffected by rapamycin, mTORC2 was shown to be affected by long-term rapamycin exposure. In addition, studies have shown that through multiple downstream signaling pathways, it acts as an autophagy inhibitor like mTORC1 [21]. Since mTORC2 is involved in cell migration, cytoskeletal reorganization, and cell survival and clearly has a role in neurite elongation and autophagy by phosphorylation of Becilin-1, GFAP, VDAC1 and FOXO family, it seems research on these mTOR proteins are crucial for understanding neuronal regeneration and mechanisms of axonal guidance.

1.9 Autophagy for reversing the process of degeneration

Research into the restoration of autophagic flux as a treatment option in the cochlea has given promising results. The interplay between autophagy and cochlear conditions is becoming more elucidated [47]. Currently, the most concrete conclusions are that any form of ototoxic damage in the form of noise-induced damage, ototoxic drugs, and aging can be alleviated or completely reversed by inducing autophagy through rapamycin, TEFB, and PRDX1 up-regulation. The most relevant results for our research come from multiple studies of restoring SGN health through autophagy induction [12, 55, 56]. The focus of such research has been the pushing back of SGN degeneration, where the effect of “homeostatic” autophagy induction was not shown to be significant or conclusive for the dosages used by autophagy inducers. Overactivation of

autophagy through its inducers showed significant morphological changes in neurite length reduction, changes in the soma size, and a reduction in supporting cell numbers (glial cells). We theorized that the induction of autophagy through minor damage caused by pulsed EMF stimulation and smaller doses of rapamycin could promote neonatal SGN health and outgrowth. More specifically, we assessed and compared morphological changes in the neonatal SGN *in - vitro* cultures due to the application of pulsed EMF stimulation and rapamycin-induced autophagy.

2 Methods and materials

2.1 Experimental design

The experiments in this study are designed to examine autophagy induction in SGN *in-vitro* cultures grown in the presence of a pulsed EMF, where varying concentrations of rapamycin, an autophagy inducer, were used. The general experimental design of the study is shown in Table 1. It is a 2x4 factorial design, resulting in eight experimental conditions. The effects were compared with a control group (without rapamycin or EMF). The concentrations for the autophagy induction assay were chosen according to literature and experimental observations with overactivating concentration for SGNs (5 μM), normally activating concentration (0.5 μM), and sub-activating concentration (0.05 μM).

Table 1. *General experimental design, overview of control and experimental groups*

	No rapamycin (R-)	**+ Rapamycin (0.05 μM) (R+L)**	**+Rapamycin (0.5 μM) (R+M)**	**+Rapamycin (5 μM) (R+H)**
No EMF (EMF-)	Control	Sub-activation control	Normal activation control	Overactivation control
EMF (EMF+)	EMF only	EMF + Sub-activation	EMF + Normal activation	EMF + Overactivation

2.2 SGN isolation

In this study, postnatal P5 Sprague-Dawely rat pups were used in the study, following the ethical and practical approval of all experimental procedures by the University of Split School of Medicine Animal Care and Use Committee as Ministry of Agriculture of Republic of Croatia (Class. 00308/15-03/0001). The isolation and culturing process was done following previous works of the lab [15, 33, 57]. After decapitation of the rat pups anesthetized on ice, the brains were removed through a mid-sagittal incision, after which the temporal bone was extracted. Then, otic capsules were dissected, and the cochlea isolated under a surgical microscope. The organ of Corti and modiolar cartilage were removed and the spiral ganglia collected. The dissection buffer was changed after each step of isolation, and it consisted of phosphate buffer saline (PBS) along with 0.3 % bovine serum albumin (BSA, Sigma-Aldrich, St. Louis, Missouri, US, catalog number #A9647) and 0.6% glucose (Merck, Kenilworth, NJ, USA, catalog number #1.04074.0500).

2.3 *In-vitro* SGN culture

The SGN explant was first treated with 500 µl of 0.25 % trypsin-EDT and with 38 U/ml DNase for dissociation at 37 °C for a duration of 30 mins. To stop the trypsinization reaction, 500 µl of DMEM:F12 medium with 10% Fetal Bovine Serum (FBS) was added. After, trituration was performed with 1000 µL and 200 µL pipette tips with around 20 suctions per tip. The suspension above was centrifuged at 1000 rpm for 5 min. The cell pellet was then resuspended in Neurobasal A medium containing 2% B27-supplement, 30 ng/ml GDNF, and 1% Pen/Strep. A Bürker-Turk chamber was used for cell counting. Afterward, cell seeding was done in 100 µL wells at 15000 cell/well density for a less dense culture. Then, the cells were cultivated on glass coverslips for 1-2 h already split into experimental and control groups in (Table 1.)

2.4 EMF stimulation

In this experiment, a time-varying magnetic field produced by custom-made copper coils placed around the cell cultures was applied for all 3DIV of growth. The coils are made with 80 turns and a diameter of 4.1 cm; a sawtooth wave signal (Fig. 5A) was applied with a current amplitude, rising pulse length, length of time between pulses, and a direction shown in Fig. 5B. The EMF stimulator device, seen in Fig. 5C, consists of the battery input, the microprocessor, and the coil. Faraday's law states that changing magnetic flux, caused by changing the electrical current amplitude, induces an electromagnetic field (EMF) in the space containing the culture medium (Fig. 6). Electric field lines are concentric to the coil loop. The neurons are affected by tangential values of concentric electric field lines (Fig. 6). The generated fields and pulse were confirmed using an oscilloscope, and the batteries were changed every 12 hours to ensure uniform stimulation.

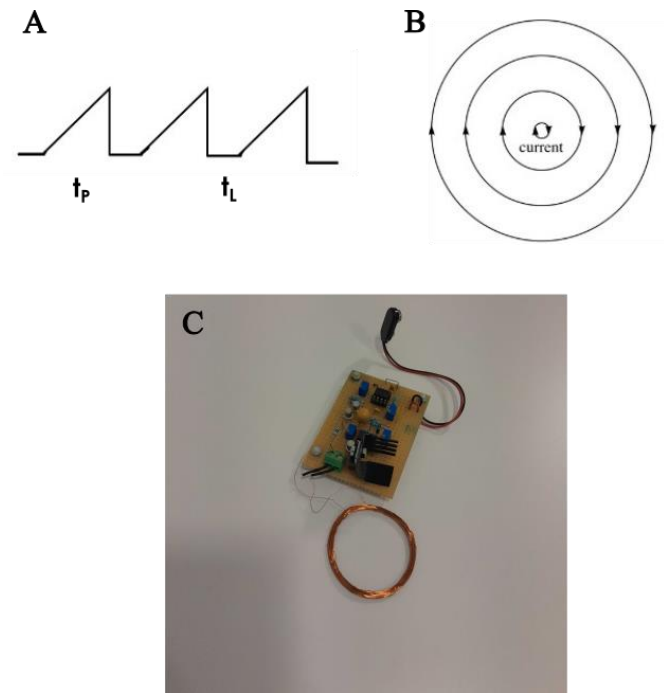

Figure 5. A) *The shape of pulsed current signal used,* ***B)*** *The used current direction, and* ***C)*** *the experimental setup of stimulating device*

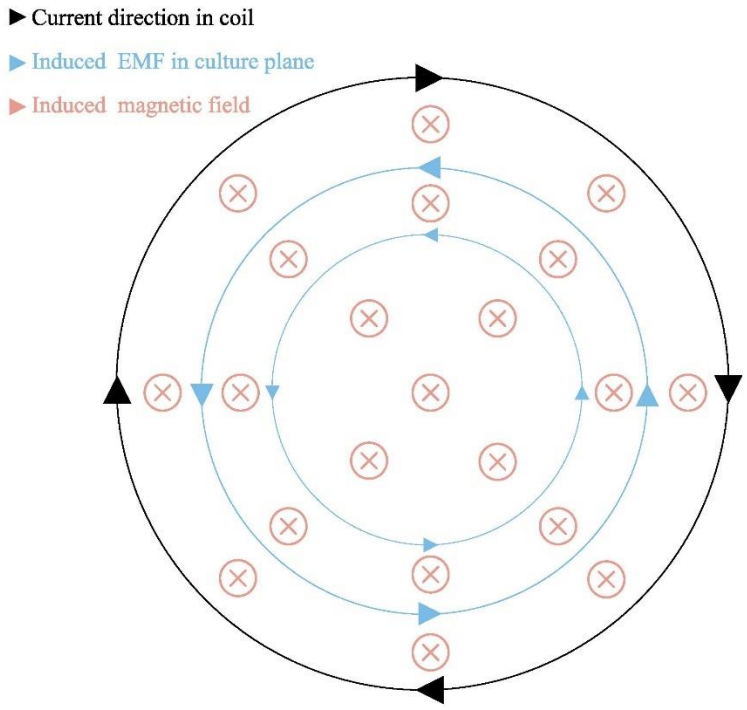

Figure 6. *Schematic representation of the electromagnetic fields generated in the culture*

2.5 Immunocytochemistry & staining

All the experiment groups had their medium changed every 24 hours along with appropriate doses of rapamycin, and after 3 DIV growth the cells were stained with LC3-II co-localizing dye, the autophagy marker (Autophagy Assay Kit, abcam, ab139484), and with a nuclear stain

(hoechst 33342, ab139484) supplemented with after which the cells were incubated for 30 min with 5 % fetal goat serum (FGS). After incubation, the cells were fixed with 4 % formaldehyde and washed 3 times. After fixation, primary antibody staining was preformed, where primary antibodies bind to the specific proteins of interest. First, the cells were permeabilized with 0.1 % Triton X-100 for 5 minutes to make the cell membranes permeable, allowing antibodies to access intracellular targets. They were then incubated in PBS containing 1% normal goat serum (NGS) for 1.5 hours at room temperature to block non-specific binding sites. The primary antibodies used for the overnight incubation were Anti-Beta III Tubulin (Tuj), mouse monoclonal at 1:500 for positive neuron identification and Anti S-100, rabbit polyclonal at 1:500 for the positive identification of glial supporting cells. After the cells were washed with 1x PBS three times, secondary staining was performed for 1.5 h. The secondary antibodies used were Alexa Fluor 568 goat anti-mouse binding to Anti-Beta III Tubulin and Alexa Fluor 647 anti-rabbit binding to Anti-S100, both antibodies were diluted to 1:500 with PBS + 1% NGS.

2.6 Fluorescence microscopy imaging

The imaging of immunocytochemically stained cell cultures was made with fluorescence microscopy, using Zeiss Axio Examiner.Z1 fluorescence microscope (Carl Zeiss AG, Oberkochen, Germany) equipped with a Colibri 7 LED fluorescence illumination system and an Iris 9 camera. The Axio Examiner.Z1 was also supplemented with a motorized stage (MT-1078/MT-2078/MT-2278, Sutter Instrument, Novato, CA, USA) suitable for precise positioning and high-resolution imaging. This custom imaging setup was managed using the μManager (Micro-Manager) software (Open Imaging, Inc., San Francisco, CA, USA) with an automatic tile-scan custom script to capture most of the sample while imaging at 10x magnification. Hoechst 33342, a marker for cell nuclei, was excited using a 385 nm UV laser, with emission collected in the blue-light range, FITC-like autophagy marker was excited using a 488 nm laser, with emission collected in the green-light range, Alexa 568, bound to neuronal tissue (Tuj), was excited using a 555 nm laser with emission collected in orange-red light range and Alexa 647, bound to glial cells (S100), was excited using a 630 laser with emission collected in red-light range. The filter set used for all imaging was 90 HE LED (Zeiss).

2.7 Image analysis

KARMENscience image processing software (Bedalov d.o.o, Kaštel Sućurac, Croatia) was used for high-throughput automatic identification and segmentation of SGNs detected on images, for neuronal tracing, as well as for the analysis of neuronal morphology parameters such as neurite length, number of neurons, cell soma size (largest drawn circle in the cell body) and neurite orientation. In addition, ImageJ (National Institutes of Health, Bethesda, MD, USA) was used for manual corrections, colocalization, and intensity analysis in very dense cell cultures.

2.8 Statistical methods

The statistical analyses were performed with custom-made scripts based on a combination of Microsoft Excel and Python programming platforms. Morphological data were presented as mean with their corresponding standard error, based on large-scale samples. In general, the data did not follow normal distributions; thus, non-parametric Kruskal-Walli's tests were used, followed by Dunn's posthoc pairwise tests between each group for measures of autophagy intensity assay, neurite outgrowth, and soma size. A proportions z-test was used to compare the ratios of developed neurons and total neurons between the groups. The values of $\mathbf{p} < 0.05$ were deemed as statistically significant.

3 Results

In this study, each sample was visualized using a 10x objective of the fluorescence microscopy, obtaining at least 5 images per sample; the imaging regions were selected randomly, making sure not to overlap them by tracking the image coordinates. The process was repeated until the appropriate number of images was obtained. We used the KARMENscience platform (Bedalov d.o.o., Kaštel Sućurac) to identify and segment neuronal cell structures visible in fluorescence images. First, the images were processed for intensity in the green channel (Fig. 7A). Next, the neuronal soma was identified and segmented into vectorized objects, allowing the calculation of the mean intensity for each pixel of the segmented objects. Each neuron's cell body area was calculated as the area of the largest possible circle encircling the soma (Fig. 7B). Also, the mean soma radii were calculated. For neurite tracing, we used a manually based ImageJ plugin Simple Neurite Tracer (SNT), as the number of images was not large enough to perform a machine-based automatic neurite tracing in KARMENscience. The mean neurite length was calculated in pixels and then converted to micrometers for all samples (Fig. 7C). The number of developed (having at least one visible neurite extruding from the cell body) and undeveloped neurons (without visible neurites extruding from the cell bodies) was counted using KARMENscience and manual identification, where a final measure of total number of neurons (developed and undeveloped SGNs) was found and a ratio of developed and total neurons could be found for each image and group.

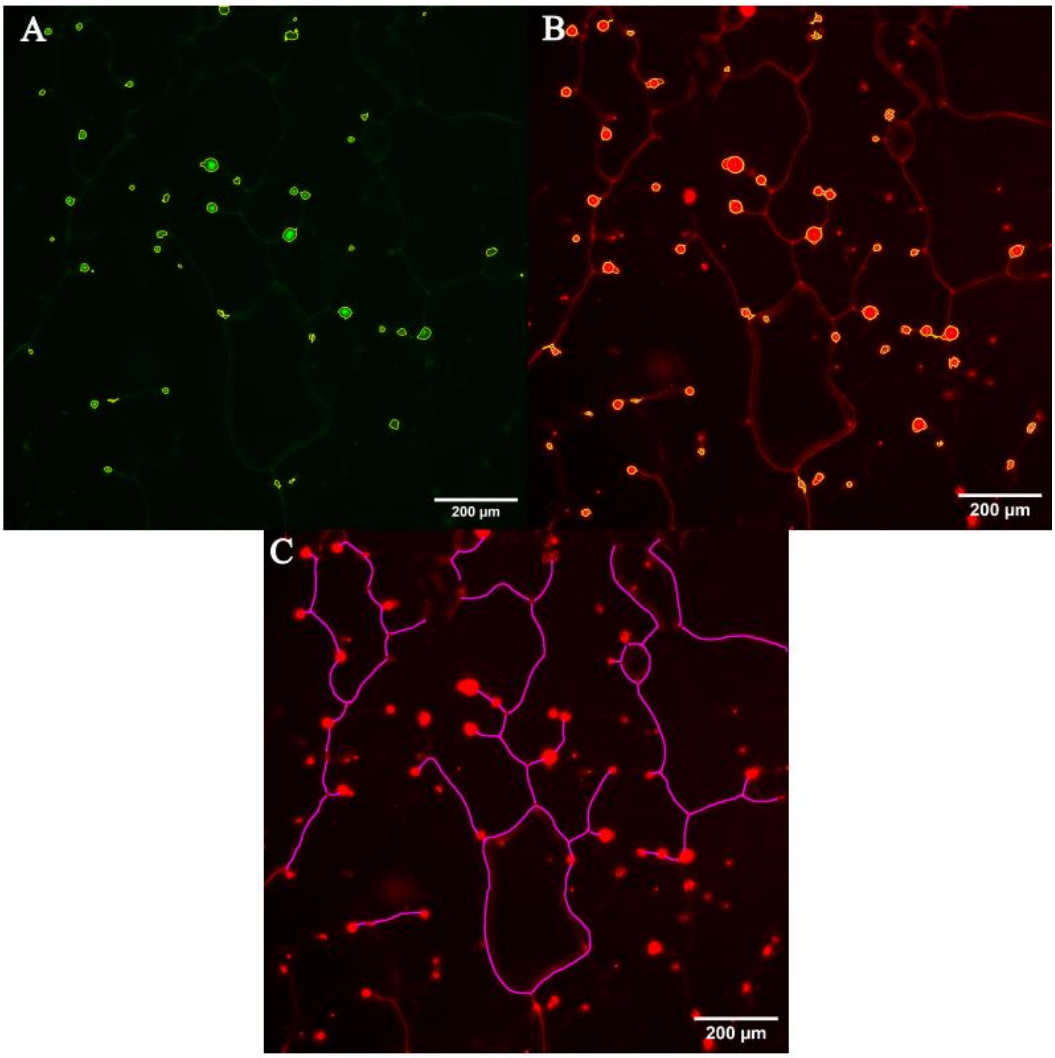

Figure 7. A) *Representative image of intensity analysis using KARMENscience,* ***B)*** *Example of soma size analysis done with KARMENscience,* ***C)*** *Example of neurite tracing done with SNT for neurite length analysis*

3.1 Autophagy is upregulated in SGNs stimulated with a pulsed EMF

The first examined parameter was the comparison of relative measures of autophagy induction between the control (C), the experimental (EMF+) and positive control (R+) groups. After 3 DIV growth, the cultures were stained, fixed, and then immunocytochemically labeled. Representative images used for LC3-II intensity analysis can be seen in Fig. 8A. A Kruskal-Walli's test was performed, and we found a statistically significant difference between the examined groups ($\boldsymbol{H} = 271.1756, \mathbf{p} < 0.001$). Relative intensity comparison showed that the amount of fluorescence intensity was increased in the EMF stimulated experimental groups

compared to the control group in almost all cases (Fig. 8B). For pairwise analysis, Dunn's post-hoc test was done, which revealed that all the differences between control and EMF stimulated groups were statistically significant except for the experimental groups treated with a sub-activating dosage of rapamycin (Appendix A1) ($\mathbf{p} > 0.05$). Further pairwise comparisons (Fig. 8C) also showed a statistically significant difference between all groups with different concentrations of rapamycin within the same experimental group (EMF treated or non-EMF treated). The final mean intensity values can be seen in (Table 2).

Table 2. *Table of all calculated means of relative intensities for the autophagy induction assay, and their respective standard errors, and sample size (N)*

	Rapamycin conc. [µM]	**Mean**	**SEM**	**N**
Control	0.05	**11027**	193	271
	0.5	**12432**	145	554
	5	**12095**	133	435
	0	**9994**	110	322
EMF	0.05	**11109**	213	264
	0.5	**15302**	477	214
	5	**13864**	420	207
	0	**11100**	153	469

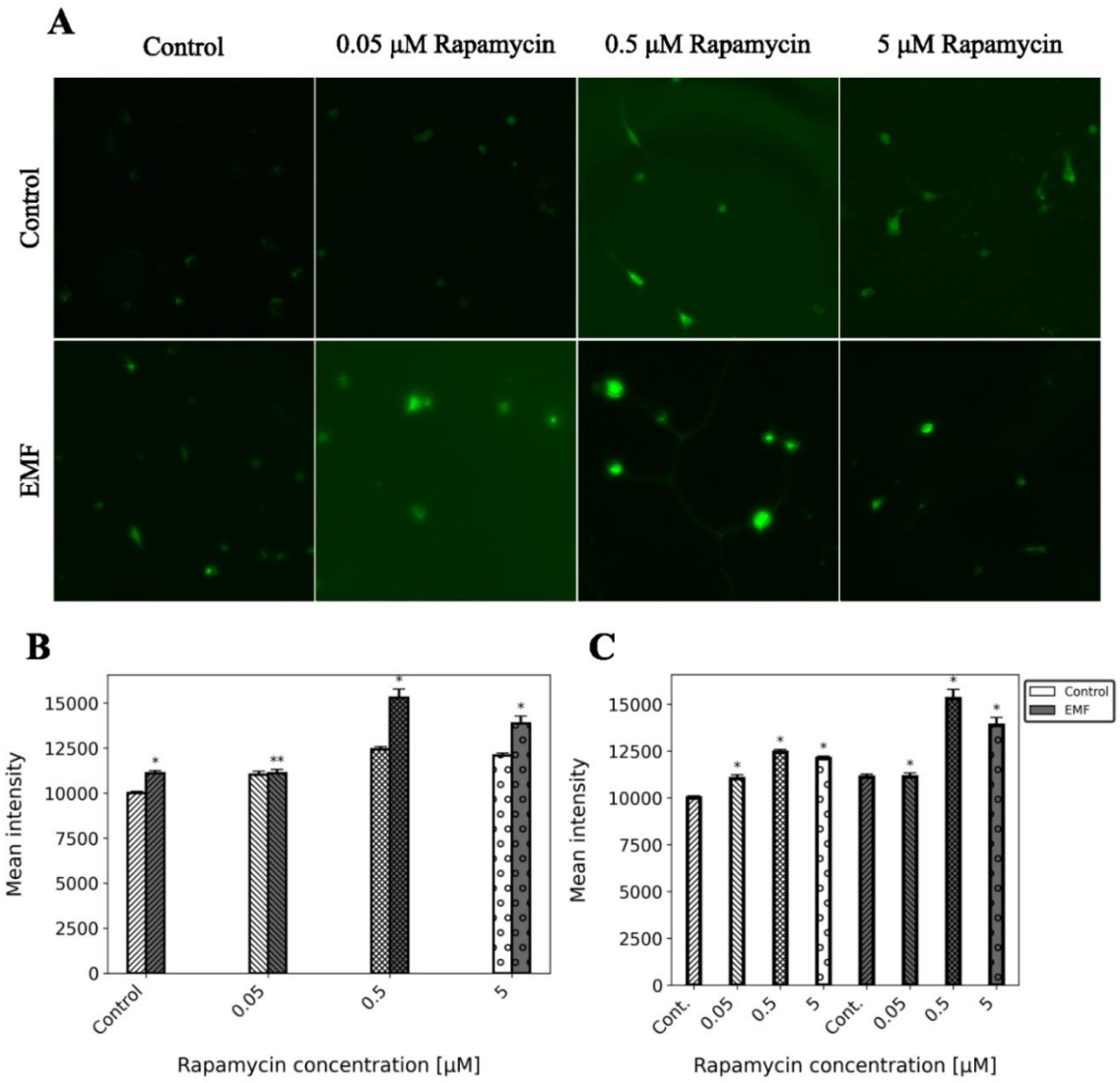

Figure 8. *Results of autophagy induction assay* ***A)*** *Representative regions of the appropriate experimental group fluorescent images of SGNs labeled with the LC3-II co-localizing autophagy marker,* ***B)*** *A comparison of relative mean intensity between EMF and non-EMF treated cultures, all data are represented as mean ± SEM, * $P < 0.05$, ** $P > 0.05$ (Not significant) from their respective non-EMF treated control groups,* ***C)*** *Calculated relative mean intensity for each group cultures, a comparison of rapamycin concentrations, all data are represented as mean ± SEM, * $P < 0.05$ from their respective control groups (Cont. groups)*

Our results indicate that EMF stimulation can indeed upregulate autophagy in SGNs where the mean fluorescence intensity from the non-rapamycin treated control group intensity (Mean=9995) was significantly increased in the non-rapamycin EMF treated group (Mean= 11100.87812). Furthermore, a combination of EMF and rapamycin at 0.5 μM and 5 μM seemed to increase the signal intensity the most (means changed from 12433 to 15302 and from 12095 to 13865 respectively). Relative intensity increased with increasing rapamycin dosage as expected where at 5 μM of rapamycin where it had a lower mean than in the 0.5 μM treated groups, likely due to SGN damage. The only non-significant difference was the comparison of the experimental groups treated with 0.05 μM of rapamycin in the EMF (Mean=11109) and non-EMF (Mean= 11028) treated groups. The comparison between positive controls of rapamycin at 0.05 μM and 0.5 μM also showed similar values (Mean=11028, Mean=12433) to the EMF stimulated group not treated with Rapamycin (Mean=11100.87812) indicating that autophagy induction via. EMF is similar to Rapamycin treatment within the range between 0.05 μM and 0.5 μM.

3.2 Neurite outgrowth is increased in EMF-stimulated SGN cultures dosed with Rapamycin

Next, a neurite outgrowth assay was performed on all groups; following the identification of SGNs and preprocessing, the neurites were labeled and segmented using a combination of automatic and manual identification using SNT (Simple Neurite Tracer Plugin, Fiji) and KARMENscience. Representative fluorescent images used for average neurite length analysis can be seen in Fig. 9A. A Kruskal-Wallis' test was performed again for non-normally distributed data. We found that there is a statistically significant difference between the examined groups ($\boldsymbol{H} = 178.7718, \mathbf{p} < 0.001$). For pairwise analysis, Dunn's post-hoc test was done, which revealed that some of the differences between control and EMF stimulated groups were statistically significant (Fig. 9B, Appendix A2). On the contrary, no statistically significant differences were found between groups treated with a sub-activating dosage of rapamycin and between those treated with an over-activating dosage. Pairwise comparisons between groups treated with different rapamycin concentrations within the same condition (EMF treated or non-EMF treated; Fig. 9C) showed a statistically significant difference between all groups with different concentrations of rapamycin except for the comparison of the EMF stimulated groups with a sub-activating concentration of rapamycin (0.05 μM). The final mean values can be seen in Table 3. Surprisingly, results showed a statistically significant decrease in the mean neurite length in the no-rapamycin groups when stimulating with an EMF, with a decrease from 64 μm (EMF-) to 48 μm in the EMF+ group ($\mathbf{p} < 0.001$), contradicting our previous results. However, in rapamycin-treated groups, EMF stimulation produced a significant increase in the mean neurite length only in the groups treated with 0.5 μM

rapamycin, where an increase from 94 μm to 133 μm was found ($\mathbf{p} < 0.001$). When comparing the effects of different rapamycin concentrations within the same condition (EMF and non-EMF treated groups) it was found that rapamycin alone decreased the mean neurite length for 0.05 μM and 5 μM groups which is consistent with previous works [12]. Importantly, a 0.5 μM dose of rapamycin alone significantly increased the mean neurite length from 64 μm to 94 μm ($\mathbf{p} < 0.05$). On the other hand, the groups treated with EMF and rapamycin showed an increase in 0.5 μM and 5 μM groups with an increase from 48 μm to 133 μm ($\mathbf{p} < 0.05$) and 78 μm ($\mathbf{p} < 0.05$) respectively.

***Table 3**. Table of calculated mean neurite length for all groups, and their respective standard errors, and sample size (N)*

	Rapamycin conc. [μM]	Mean [μm]	SE	N
Control	0	**64**	7	67
	0.05	**58**	3	432
	0.5	**94**	6	140
	5	**61**	4	49
EMF	0	**48**	3	95
	0.05	**55**	3	82
	0.5	**133**	8	162
	5	**78**	6	192

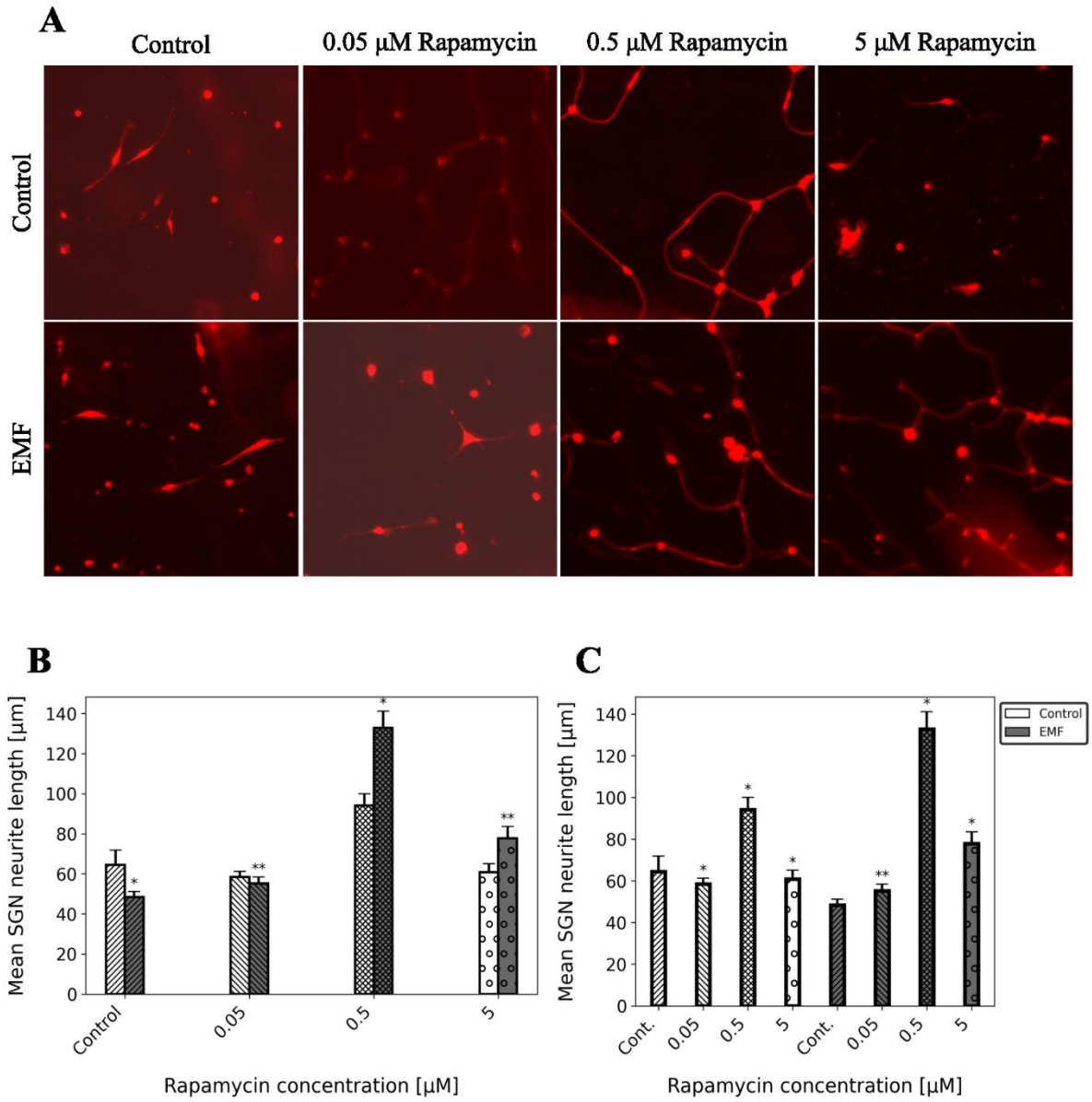

Figure 9. *Results of mean neurite length assay* ***A)*** *Representative regions of the appropriate experimental group fluorescent images of SGNs showing neuronal tissue, labeled with TUJ1 primary antibody bounded with Alexa 568 fluorophore* ***B)*** *A comparison of mean neurite length between EMF and non-EMF treated cultures, all data are represented as mean ± SEM,* $* P < 0.05$, $** P > 0.05$ *(Not significant) from their respective non-EMF treated control groups,* ***C)*** *Calculated mean neurite length for each group, a comparison of Rapamycin concentrations, all data are represented as mean ± SEM,* $* P < 0.05$, $** P > 0.05$ *(Not significant) from their respective control groups (Cont. groups).*

3.3 Neuron soma size is affected by autophagy induction and EMF

Next, the effect of treatments on average soma radii was assessed. The analysis was done on the same image sets used for neurite length analysis (Fig. 10A), with additional image analyses to identify a circular body, defined as the largest possible circle drawn inside the cell soma. These measurements were used to calculate soma radii for all neurons in all groups as a relative measure of cell soma size. First, a Kruskal-Wali's test was used to determine if there was a significant difference in soma radius between all the groups. We found a significant difference between the groups ($\boldsymbol{H} = 183.2603, \mathbf{p} < 0.001$). As before, in the pairwise comparison analysis, Dunn's post-hoc test revealed that all the EMF-treated groups showed a significant difference in soma radius compared with their EMF- groups except for the groups with no rapamycin showing insignificant differences ($\mathbf{p} > 0.05$) (Fig. 10A; Appendix A3). The 0.05 μM rapamycin-treated group showed an increase from 4.1 μm to 5.6 μm when treated with EMF ($\mathbf{p} < 0.05$) and the 0.5 μM treated group showed an increase from 3.9 μm to 4.8 μm when treated with EMF ($\mathbf{p} < 0.05$). As expected, the group treated with an over-activating concentration of rapamycin (5 μM) showed a significant decrease in mean soma radius, from 4.5 μm to 3.3 μm ($\mathbf{p} < 0.05$). As for the pairwise comparisons of the effect of different rapamycin concentrations within the same group, the results showed that among groups not treated with EMF, no significant difference was found in soma size with increasing rapamycin concentrations (Fig. 9B, Appendix A3). In the case of groups treated with an EMF, varying concentrations of rapamycin showed a significant effect on SGN soma size. Surprisingly, the largest increase was observed in the 0.05 μM rapamycin-treated group, from 3.7 μm for the control group to 5.55 μm ($\mathbf{p} < 0.001$) for the mean soma radius, followed by a smaller increase to 4.8 μm ($\mathbf{p} < 0.001$) for the 0.5 μM treated group, and finally, the 5 μM rapamycin-treated group showed a reduced mean soma radius at 3.3 μm ($\mathbf{p} < 0.001$). A summary of these results can be seen in Table 5. Our results show that the effects of EMF alone are inconclusive; however, when combined with rapamycin, larger cell bodies are observed. The over -activating concentrations showed a significant decrease, further amplified by EMF. No evidence was found of rapamycin alone affecting soma size.

Table 4. *A summary of calculated mean radii of SGN soma for all experimental groups*

	Rapamycin conc. [µM]	Mean [µm]	SE	N
Control	0	**4.1**	0.1	131
	0.05	**4.1**	0.1	277
	0.5	**3.9**	0.1	55
	5	**4.5**	0.2	47
EMF	0	**3.7**	0.1	63
	0.05	**5.6**	0.2	56
	0.5	**4.8**	0.2	151
	5	**3.3**	0.2	63

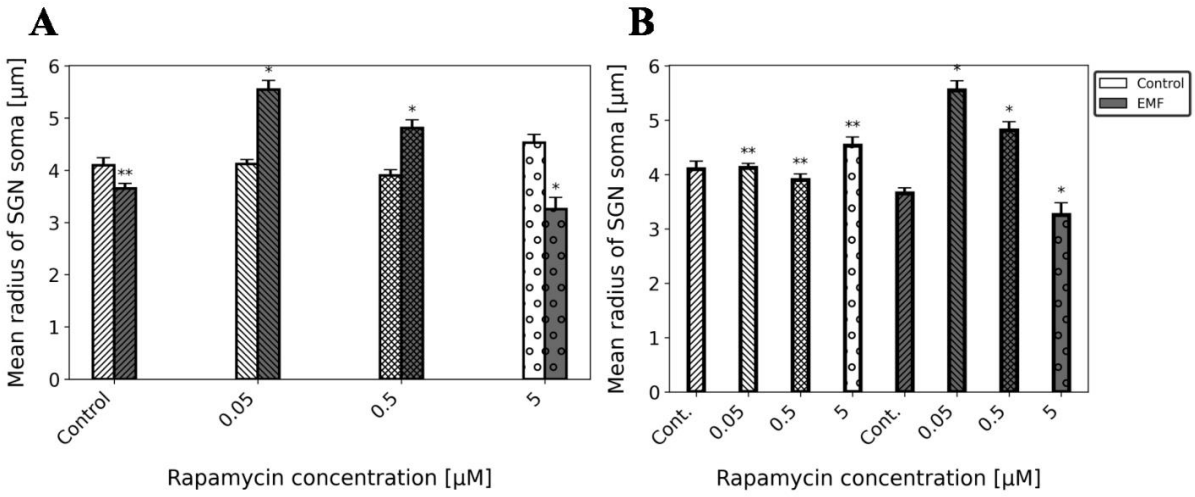

Figure 10. *Visualization of soma radius analysis results* ***A)*** *A comparison of the effects of EMF stimulation on the soma radius of cultures treated with the same dose of rapamycin, all data are represented as mean ± SEM, * $P < 0.05$, ** $P > 0.05$ (Not significant) from their respective non-EMF treated control groups,* ***B)*** *Calculated mean cell soma radii for each group, a comparison of rapamycin concentrations, all data are represented as mean ± SEM, * $P < 0.05$, ** $P > 0.05$ (Not significant) from their respective control groups (Cont. groups).*

3.4 EMF stimulation and rapamycin modulate the rate of SGN maturation

Finally, we aimed to examine how different treatment conditions affect the differentiation and development of SGNs. To this end, the number of all nuclei was calculated for all images and groups. Following this, the number of developed neurons (defined as having at least one visible neurite with the minimal length of 10 μm) was calculated for each image (Appendix B). A proportions z-test was used (Appendix A4) to determine significant differences between the proportions of developed neurons in all experimental groups. The EMF treatment alone did not significantly change the proportion of developed neurons, as seen in (Fig. 11A) ($\boldsymbol{Z} = -1.7539$, $\mathbf{p} > 0.05$), having shown a very small increase. The rest of the comparisons between EMF and non-EMF-treated groups showed curious results. First, for a low concentration of rapamycin (0.05 μM), EMF treatment seemed to interfere with the positive effect of rapamycin at this concentration, causing a significant decrease from 0.56 to 0.18 ($\boldsymbol{Z} = 9.7467$, $\mathbf{p} < 0.001$). As for the moderate and high concentrations of rapamycin (0.5 μM and 5 μM) the results seem to follow trends from previous analysis, that of a synergistic effect between rapamycin and EMF stimulation, increases from 0.29 to 0.51 ($\boldsymbol{Z} = -5.7349$, $\mathbf{p} < 0.001$) and from 0.09 to 0.48 ($\boldsymbol{Z} = -11.1234$, $\mathbf{p} < 0.001$), respectively. As for the comparisons of the effect of rapamycin concentration alone (Fig. 11B), for the non-EMF treated group, the small and moderate concentrations of rapamycin increased the proportion of developed neurons significantly from 0.09 to 0.56 ($\boldsymbol{Z} = 16.0538$, $\mathbf{p} < 0.001$) and 0.29 ($\boldsymbol{Z} = 7.4773$, $\mathbf{p} < 0.001$) , respectively. A high concentration of rapamycin seemed to not have a significant effect on this proportion ($\boldsymbol{Z} = 0.1196$, $\mathbf{p} > 0.05$). In the case of the EMF treated group, the use of rapamycin yielded a significant increase from the control group at 0.13 ratio of developed neurons, the increase was to 0.18 for the 0.05 μM treated group ($\boldsymbol{Z} = 1.9831$, $\mathbf{p} < 0.05$), to 0.51 for the 0.5 μM treated group ($\boldsymbol{Z} = 11.5613$, $\mathbf{p} < 0.001$) and to 0.48 for the 5 μM treated group ($\boldsymbol{Z} = 10.0163$, $\mathbf{p} < 0.001$). A summary of the results can be seen in Table 5.

Table 5. *A summary of calculated mean proportions of detected developed SGNs to all detected SGNs, with corresponding statistics, * the number of samples here is indicative of the amount of images per sample, the specific counts for each image can be found in (Appendix B)*

	Rapamycin conc. [μM]	Mean	SE	N*
Control	0	**0.09**	0.01	6
	0.05	**0.56**	0.02	5
	0.5	**0.29**	0.03	5
	5	**0.09**	0.01	8
EMF	0	**0.13**	0.02	7
	0.05	**0.18**	0.02	6
	0.5	**0.51**	0.03	5
	5	**0.48**	0.03	5

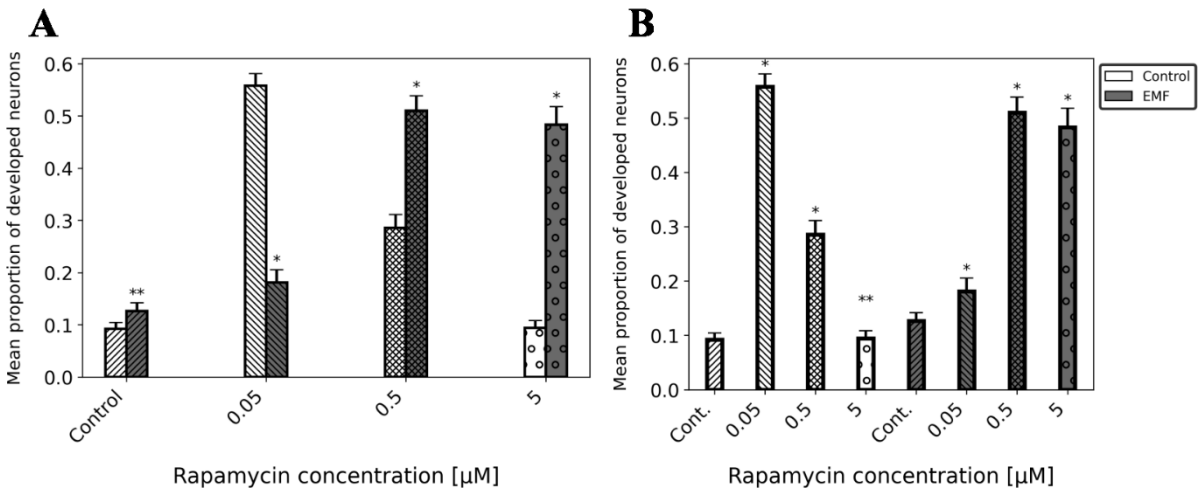

Figure 11. *Summary of results for comparison of proportion of developed neurons against all neurons* ***A)*** *A bar plot showing the comparison of non-EMF and EMF treated groups with the same rapamycin concentration, all data are represented as mean ± SEM,* $* P < 0.05$, $** P > 0.05$ *(Not significant) from their respective non-EMF treated groups,* ***B)*** *Bar plot comparison of effects of different rapamycin concentrations on mean proportion of developed neurons from their respective control groups (Cont. Groups), all data are represented as mean ± SEM,* $* P < 0.05$, $** P > 0.05$ *(Not significant) from the control groups with the same condition (Cont. Groups)*

4 Discussion

The present study aimed to examine the effects of autophagy induction and EMF on the growth and size of neonatal SGNs. To this end, rapamycin was administered in most control groups besides EMF and was replenished for each medium change during 3 DIV. In our case, Rapamycin served not only as a positive control for autophagy but as a parameter to be examined due to observed potential synergistic effects with EMF stimulation. Before analysis of the effects of autophagy induction, it is essential to consider that at different developmental stages, autophagic and apoptotic activity can vary intensely, especially in the P1 to P7 window, and the rats used were P5. Specifically, a study found that SGNs of neonatal rats at around P5 experience increasing levels of autophagic and apoptotic activity (Type I cell death) [49], this should be taken into consideration when comparing our results.

Firstly, it is clear that EMF successfully induced autophagy, and in comparison, with positive controls with rapamycin, it seems the effect is not as large as that of autophagy induction via higher concentrations of rapamycin. Furthermore, further evidence that EMF influences autophagy can be seen in groups treated with both EMF and rapamycin, which showed an even greater level of autophagic activity. Of course, this is only a relatively qualitative measure since the amount of autophagosomes depends on their production and degradation rate. For a more robust measure, autophagic flux should be assessed in the future by inhibition of lysosome activity to ensure that the observed increase is indeed only autophagy induction.

The most significant parameter that was examined is the mean SGN neurite length, which showed surprisingly insignificant results when treated with EMF alone, this contradicts some of our previous results and could be caused by changes in the culture conditions such as cell density, medium composition and EMF stimulation duration which were all different for these experiments, this analysis should be repeated with standardized conditions. Rapamycin treatment, on the other hand, showed a significant increase in neurite length for the medium concentration and the most significant increase in combination with EMF stimulation, implying a synergistic effect between EMF and rapamycin for medium concentrations. High concentrations of rapamycin showed either a smaller increase or even a decrease in neurite length, which is to be expected, as 5 μM is usually the threshold where autophagy induction starts being excessive, and Type II (Autophagic) cell death can start occurring. Smaller concentrations of rapamycin showed negligent effects on neurite length.

As for soma radius, EMF and rapamycin alone showed no significant effects; the only significant increases were in the groups with combined conditions with an increase for small and medium concentrations, with high concentration again showing a surprising reduction in soma size. Among these 3 parameters, a similar trend can be noticed: smaller to medium concentrations of rapamycin, when supplemented with EMF stimulation, show a significantly greater increase in autophagic activity, SGN size, and outgrowth. Besides electrical or

mechanical effects, this interplay between EMF and intracellular signaling might be through ROS generation, which, besides causing more oxidative stress and damage, also induces more autophagy, as previously reported [40]. However, minor damage doesn't seem to cause cell death with these parameters; in fact, adding rapamycin appears to boost autophagy further. Thus, we theorize that this observed trend is in the form of a „preconditioning" effect, a cellular response to oxidative stress reported to be a potential neuroprotective strategy [58]. So, a combination of autophagy induction and ROS signaling, which induces more mitophagy and the release of anti-apoptotic factors, causes the observed effect of more significant SGN development. Another observed trend is the decrease in the observed preconditioning effect or outright detrimental effects in the groups supplemented with a high concentration of rapamycin, this is likely due to autophagy over-activation. These promising results should, in the future, be examined by assessing ROS generation directly, along with other protein markers for cell viability and autophagy as to determine whether this could indeed be a usable strategy for promoting SGN health during development.

The analysis of the proportion of developed neurons showed a different trend in the case of a low dosage of rapamycin, where EMF seems to have a negative effect on the number of developed SGNs. Otherwise, the synergistic effect was again observed in the groups with medium and high doses of rapamycin. In general, autophagy induction via rapamycin seems to have a positive effect on neuronal development in smaller doses of rapamycin, while for higher it seems to have a detrimental effect; previous studies showed detrimental effects of high rapamycin. However, the positive effects were limited to restoring function in the face of damage [11, 55]. On the other hand, EMF stimulation seems to increase development for higher doses of rapamycin, which could indicate that EMF stimulation causes more complex effects than just autophagy induction since EMF combined with rapamycin should show similar results to rapamycin only group (5 μM). Still, the opposite seems to be the case. Due to the high variability of the number of developed neurons, which could be attributed to different sources of unintentional stress or parts of the explant taken for the culture, this result should be carefully interpreted and further examined by a higher number of experiments to reduce the chances of unintentional false positives. Likewise, since a significant part of image analysis was manual corrections, some results may vary due to human error.

5 Conclusion

Numerous methods for guiding and promoting neuron outgrowth have been developed, and it is an ongoing topic of research on how to utilize these findings to treat SNHL applications. In this study, we propose a new approach to support the growth of developing SGNs for improving cochlear implant efficiency. The first step in this new potential application was identified: using electromagnetic guidance cues in tandem with autophagy induction can have a synergistic effect of promoting SGN health, outgrowth, and development larger than any of these parameters alone, where cases of autophagy overactivation caused a reduction in overall SGN development. Furthermore, our work demonstrated that autophagy, as an intracellular process, is closely linked with SGN growth, and its manipulation can significantly affect critical morphological parameters such as neurite outgrowth, soma size, and the number of developing neurons. Our findings might indicate that autophagy is not simply a side effect of neuronal growth but one of the main driving forces. Yet, there is evidence that EMF stimulation alone might not have such straightforward consequences as autophagy induction alone in terms of intracellular signaling and should be carefully investigated in the future due to the synergistic effect persisting in autophagy over-activating groups. The effects of pulsed EMF stimulation alone did not show significant differences in neuron outgrowth or size, perhaps due to a smaller sample size, and should be examined further. Due to the sensitive nature of research linked with cellular stress responses like this, more parameters such as autophagic flux, multiple autophagy proteins, cell viability, and ROS generation should be examined to correctly pinpoint intracellular signaling caused by EMF and the best possible parameters for utilizing this combined approach.

6 References

1.

[1] M. T. J. Halma, P. E. Marik, and Y. M. Saleeby: *Exploring Autophagy in Treating Spike Protein-related Pathology*, 2023. DOI: 10.20944/preprints202306.1903.v1.

[2] M. R. Aburto, J. M. Hurlé, I. Varela-Nieto, and M. Magariños: *Autophagy During Vertebrate Development*, Cells, **vol. 1**, 428–448, 2012. DOI: 10.3390/cells1030428.

[3] T. Yonekawa and A. Thorburn: *Autophagy and cell death*, Essays in Biochemistry, **vol. 55**, 105–117, 2013. DOI: 10.1042/bse0550105.

[4] L. Galluzzi, J. M. Bravo-San Pedro, B. Levine, D. R. Green, and G. Kroemer: *Pharmacological modulation of autophagy: therapeutic potential and persisting obstacles*, Nat Rev Drug Discov, **vol. 16**, 487–511, 2017. DOI: 10.1038/nrd.2017.22.

[5] L. Zhang, S. Chen, and Y. Sun: *Mechanism and Prevention of Spiral Ganglion Neuron Degeneration in the Cochlea*, Front. Cell. Neurosci., **vol. 15**, 814-891, 2022. DOI: 10.3389/fncel.2021.814891.

[6] *World Health Organization*, Deafness and Hearing Loss. URL: Deafness and hearing loss - World Health Organization (WHO)

[7] J. B. Nadol *et al.*: *Histopathology of Cochlear Implants in Humans*, Ann Otol Rhinol Laryngol, **vol. 110**, 883–891, 2001. DOI: 10.1177/000348940111000914.

[8] J. N. Fayad and F. H. Linthicum: *Multichannel Cochlear Implants: Relation of Histopathology to Performance*, The Laryngoscope, **vol. 116**, 1310–1320, 2006. DOI: 10.1097/01.mlg.0000227176.09500.28.

[9] Santaolalla F, Salvador C, Martínez A, Sánchez JM, Del Rey AS. *Inner ear hair cell regeneration: A look from the past to the future.* Neural Regen Res., **vol. 8(24)**, 2284-9. DOI: Development of the sexually dimorphic nucleus of the preoptic area and ...

[10] T. G. Landry, A. K. Wise, J. B. Fallon, and R. K. Shepherd: *Spiral ganglion neuron survival and function in the deafened cochlea following chronic neurotrophic*

treatment, Hearing Research, **vol. 282**, 303–313, 2011. DOI: 10.1016/j.heares.2011.06.007.

[11] L. Guo, W. Cao, Y. Niu, S. He, R. Chai, and J. Yang: *Autophagy Regulates the Survival of Hair Cells and Spiral Ganglion Neurons in Cases of Noise, Ototoxic Drug, and Age-Induced Sensorineural Hearing Loss*, Front. Cell. Neurosci., **vol. 15**, 760422, 2021. DOI: 10.3389/fncel.2021.760422.

[12] S. Guo *et al.: Rapamycin Protects Spiral Ganglion Neurons from Gentamicin-Induced Degeneration In Vitro*, JARO, **vol. 20**, 475–487, 2019. DOI: 10.1007/s10162-019-00717-3.

[13] B. Ye *et al.*: *Restoring autophagic flux attenuates cochlear spiral ganglion neuron degeneration by promoting TFEB nuclear translocation via inhibiting MTOR*, Autophagy, **vol. 15**, 998–1016, 2019. DOI: 10.1080/15548627.2019.1569926.

[14] V. Radotić, D. Braeken, and D. Kovačić: *Microelectrode array-induced neuronal alignment directs neurite outgrowth: analysis using a fast Fourier transform (FFT)*, Eur Biophys J, **vol. 46**, 719–727, 2017. DOI: 10.1007/s00249-017-1263-1.

[15] M. Mattotti, L. Micholt, D. Braeken, and D. Kovačić: *Characterization of spiral ganglion neurons cultured on silicon micro-pillar substrates for new auditory neuro-electronic interfaces*, J. Neural Eng., **vol. 12**, 026001, 2015. DOI: 10.1088/1741-2560/12/2/026001.

[16] J. Menardo *et al.*: *Oxidative Stress, Inflammation, and Autophagic Stress as the Key Mechanisms of Premature Age-Related Hearing Loss in SAMP8 Mouse Cochlea*, Antioxidants & Redox Signaling, **vol. 16**, 263–274, 2012. DOI: 10.1089/ars.2011.4037.

[17] Henry Gray: *Anatomy of the Human Body*, Lea & Febiger, Philadelphia, 1918.

[18] *Toppr*, URL: Organ of Corti

[19] K. D. Zhang and T. M. Coate: *Recent advances in the development and function of type II spiral ganglion neurons in the mammalian inner ear*, Seminars in Cell & Developmental Biology, **vol. 65**, 80–87, 2017. DOI: 10.1016/j.semcdb.2016.09.017.

[20] Y. C. Kim and K.-L. Guan: *mTOR: a pharmacologic target for autophagy regulation*, J. Clin. Invest., **vol. 125**, 25–32, 2015. DOI: 10.1172/JCI73939.

[21] J. Ballesteros-Álvarez and J. K. Andersen: *mTORC2: The other mTOR in autophagy regulation*, Aging Cell, **vol. 20**, e13431, 2021. DOI: 10.1111/acel.13431.

[22] S. Chatterjee, C. Munshi, and S. Bhattacharya: *The Role of mTOR, Autophagy, Apoptosis, and Oxidative Stress During Toxic Metal Injury*, Molecules to Medicine with mTOR, 69–81, 2016. DOI: 10.1016/B978-0-12-802733-2.00013-X.

[23] M. Murakami *et al.*: *mTOR Is Essential for Growth and Proliferation in Early Mouse Embryos and Embryonic Stem Cells*, Molecular and Cellular Biology, **vol. 24**, 6710–6718, 2004. DOI: 10.1128/MCB.24.15.6710-6718.2004.

[24] P. C. Roehm and M. R. Hansen: *Strategies to preserve or regenerate spiral ganglion neurons:*, Current Opinion in Otolaryngology & Head and Neck Surgery, **vol. 13**, 294–300, 2005. DOI: 10.1097/01.moo.0000180919.68812.b9.

[25] B. L. Leigh, K. Truong, R. Bartholomew, M. Ramirez, M. R. Hansen, and C. A. Guymon: *Tuning Surface and Topographical Features to Investigate Competitive Guidance of Spiral Ganglion Neurons*, ACS Appl. Mater. Interfaces, **vol. 9**, 31488–31496, 2017. DOI: 10.1021/acsami.7b09258.

[26] L. Xu, A. E. Seline, B. Leigh, M. Ramirez, C. A. Guymon, and M. R. Hansen: *Photopolymerized Microfeatures Guide Adult Spiral Ganglion and Dorsal Root Ganglion Neurite Growth*, Otology & Neurotology, **vol. 39**, 119–126, 2018. DOI: 10.1097/MAO.0000000000001622.

[27] T. G. Landry, A. K. Wise, J. B. Fallon, and R. K. Shepherd: *Spiral ganglion neuron survival and function in the deafened cochlea following chronic neurotrophic*

treatment, Hearing Research, **vol. 282**, 303–313, 2011. DOI: 10.1016/j.heares.2011.06.007.

[28] A. Markus, T. D. Patel, and W. D. Snider: *Neurotrophic factors and axonal growth*, Current Opinion in Neurobiology, **vol. 12**, 523–531, 2002. DOI: 10.1016/S0959-4388(02)00372-0.

[29] W.-Q. Zuo *et al.*: *Sensitivity of spiral ganglion neurons to damage caused by mobile phone electromagnetic radiation will increase in lipopolysaccharide-induced inflammation in vitro model*, J Neuroinflammation, **vol. 12**, 105, 2015. DOI: 10.1186/s12974-015-0300-1.

[30] L. Yao, A. Pandit, S. Yao, and C. D. McCaig: *Electric Field-Guided Neuron Migration:A Novel Approach in Neurogenesis*, Tissue Engineering Part B: Reviews, **vol. 17**, 143–153, 2011. DOI: 10.1089/ten.teb.2010.0561.

[31] A. Rotem and E. Moses: *Magnetic Stimulation of One-Dimensional Neuronal Cultures*, Biophysical Journal, **vol. 94**, 5065–5078, 2008. DOI: 10.1529/biophysj.107.125708.

[32] W.-L. Cheng and C.-C. K. Lin: *The Effects of Different Electrical Stimulation Protocols on Nerve Regeneration Through Silicone Conduits:*, The Journal of Trauma: Injury, Infection, and Critical Care, **vol. 56**, 1241–1246, 2004. DOI: 10.1097/01.TA.0000071289.11767.22.

[33] V. Radotić, A. Bedalov, P. Drviš, D. Braeken, and D. Kovačić: *Guided growth with aligned neurites in adult spiral ganglion neurons cultured* in vitro *on silicon micro-pillar substrates*, J. Neural Eng., **vol. 16**, 066037, 2019. DOI: 10.1088/1741-2552/ab2968.

[34] N. Zhang, H. Yan, and X. Wen: *Tissue-engineering approaches for axonal guidance*, Brain Research Reviews, **vol. 49**, 48–64, 2005. DOI: 10.1016/j.brainresrev.2004.11.002.

[35] K. Truong *et al.*: *Interaction of micropatterned topographical and biochemical cues to direct neurite growth from spiral ganglion neurons*, Hearing Research, **vol. 409**, 108315, 2021. DOI: 10.1016/j.heares.2021.108315.

[36] R. M. Dorrian, C. F. Berryman, A. Lauto, and A. V. Leonard: *Electrical stimulation for the treatment of spinal cord injuries: A review of the cellular and molecular mechanisms that drive functional improvements*, Front. Cell. Neurosci., **vol. 17**, 1095259, 2023. DOI: 10.3389/fncel.2023.1095259.

[37] L. Matter, B. Harland, B. Raos, D. Svirskis, and M. Asplund: *Generation of direct current electrical fields as regenerative therapy for spinal cord injury: A review*, APL Bioengineering, **vol. 7**, 031-505, 2023. DOI: 10.1063/5.0152669.

[38] Q. Liu *et al.*: *Electric field stimulation boosts neuronal differentiation of neural stem cells for spinal cord injury treatment via PI3K/Akt/GSK-3β/β-catenin activation*, Cell Biosci, **vol. 13**, 4, 2023. DOI: 10.1186/s13578-023-00954-3.

[39] M. N. Peter *et al.*: *Influence of In Vitro Electrical Stimulation on Survival of Spiral Ganglion Neurons*, Neurotox Res, **vol. 36**, 204–216, 2019. DOI: 10.1007/s12640-019-00017-x.

[40] K. Liu *et al.*: *The protective effect of autophagy on mouse spermatocyte derived cells exposure to 1800MHz radiofrequency electromagnetic radiation*, Toxicology Letters, **vol. 228**, 216–224, 2014. DOI: 10.1016/j.toxlet.2014.05.004.

[41] H. Wang and X. Zhang: *Magnetic Fields and Reactive Oxygen Species*, IJMS, **vol. 18**, 2175, 2017. DOI: 10.3390/ijms18102175.

[42] J. Zielinski, A. D. Ducray, A. M. Moeller, M. Murbach, N. Kuster, and M. Mevissen: *Effects of pulse-modulated radiofrequency magnetic field (RF-EMF) exposure on apoptosis, autophagy, oxidative stress and electron chain transport function in human neuroblastoma and murine microglial cells*, Toxicology in Vitro, **vol. 68**, 104963, 2020. DOI: 10.1016/j.tiv.2020.104963.

[43] H. Y. Hui: *Effects of Electromagnetic Radiation on Autophagy and its Regulation*, Biomed Environ Sci, **vol. 31(1)**, 57-65, DOI: https://doi.org/10.1016/S0959-4388(02)00372-0.

[44] M. Schieber and N. S. Chandel: *ROS Function in Redox Signaling and Oxidative Stress*, Current Biology, **vol. 24**, R453–R462, 2014. DOI: 10.1016/j.cub.2014.03.034.

[45] C. Lennicke and H. M. Cochemé: *Redox metabolism: ROS as specific molecular regulators of cell signaling and function*, Molecular Cell, **vol. 81**, 3691–3707, 2021. DOI: 10.1016/j.molcel.2021.08.018.

[46] J. Zhang *et al.*: *ROS and ROS-Mediated Cellular Signaling*, Oxidative Medicine and Cellular Longevity, **vol. 2016**, 1–18, 2016. DOI: 10.1155/2016/4350965.

[47] T. Zou, R. Xie, S. Huang, D. Lu, and J. Liu: *Potential role of modulating autophagy levels in sensorineural hearing loss*, Biochemical Pharmacology, **vol. 222**, 116115, 2024. DOI: 10.1016/j.bcp.2024.116115.

[48] Y. Wada, G.-H. Sun-Wada, N. Kawamura, and M. Aoyama: *Role of autophagy in embryogenesis*, Current Opinion in Genetics & Development, **vol. 27**, 60–66, 2014. DOI: 10.1016/j.gde.2014.03.010.

[49] N. Mizushima and B. Levine: *Autophagy in mammalian development and differentiation*, Nat Cell Biol, **vol. 12**, 823–830, 2010. DOI: 10.1038/ncb0910-823.

[50] O. J. Lieberman, A. F. McGuirt, G. Tang, and D. Sulzer: *Roles for neuronal and glial autophagy in synaptic pruning during development*, Neurobiology of Disease, **vol. 122**, 49–63, 2019. DOI: 10.1016/j.nbd.2018.04.017.

[51] R. Guo *et al.*: *Autophagy-Mediated Synaptic Refinement and Auditory Neural Pruning Contribute to Ribbon Synaptic Maturity in the Developing Cochlea*, Front. Mol. Neurosci., **vol. 15**, 15:850035, 2022. DOI: 10.3389/fnmol.2022.850035.

[52] S. Hou *et al.*: *Distinct Expression Patterns of Apoptosis and Autophagy-Associated Proteins and Genes during Postnatal Development of Spiral Ganglion Neurons in Rat*, Neural Plasticity, **vol. 2020**, 1–9, 2020. DOI: 10.1155/2020/9387560.

[53] W. Wu, P. Chen, J. Yang, and Y. Liu: *A Low Dose of Rapamycin Promotes Hair Cell Differentiation by Enriching SOX2+ Progenitors in the Neonatal Mouse Inner Ear Organoids*, JARO, **vol. 25**, 149–165, 2024. DOI: 10.1007/s10162-024-00938-1.

[54] S. E. Thomson *et al.*: *Microtopographical cues promote peripheral nerve regeneration via transient mTORC2 activation*, Acta Biomaterialia, **vol. 60**, 220–231, 2017. DOI: 10.1016/j.actbio.2017.07.031.

[55] W. Liu *et al.*: *PRDX1 activates autophagy via the PTEN-AKT signaling pathway to protect against cisplatin-induced spiral ganglion neuron damage*, Autophagy, **vol. 17**, 4159–4181, 2021. DOI: 10.1080/15548627.2021.1905466.

[56] B. Ye *et al.*: *Restoring autophagic flux attenuates cochlear spiral ganglion neuron degeneration by promoting TFEB nuclear translocation via inhibiting MTOR*, Autophagy, **vol. 15**, 998–1016, 2019. DOI: 10.1080/15548627.2019.1569926.

[57] T. Borić: *Morphological characterization of spiral ganglion neurons grown in the pulsating electromagnetic field*, URL: https://urn.nsk.hr/urn:nbn:hr:166:100785

[58] R. Akki *et al.*: *Neuronal-like differentiated SH-SY5Y cells adaptation to a mild and transient H_2O_2 -induced oxidative stress*, Cell Biochemistry & Function, **vol. 36**, 56–64, 2018. DOI: 10.1002/cbf.3317.

A Appendix: Complete statistics

A1 Relative intensity statistics

Table 6. *Color and number legend for statistics*

Color legend	Rapamycin conc. [µM]
non-EMF	0
EMF	0.05
	0.5
	5

Table 7. *Statistics for autophagy induction assay, relative intensity*

Group	Mean	Standard Error	N
0	9994.449509	110.7451588	271
0	11100.87812	153.8270513	554
0.05	11027.96208	193.1912461	435
0.05	11109.00014	213.1047515	322
0.5	12432.67002	145.7400772	264
0.5	15302.32217	477.5809236	214
5	12095.31203	133.3485355	207
5	13864.66297	420.009946	469

Table 8. *Shapiro-Wilk test for normalcy of data, relative intensity*

Group	Shapiro-Wilk Statistic	Shapiro-Wilk p-value
0	0.898227995	7.12048E-14
0	0.801018069	1.42492E-23
0.05	0.812756603	2.22945E-17
0.05	0.831790571	3.09576E-16
0.5	0.909017884	1.07701E-17
0.5	0.87683952	3.52392E-12
5	0.917895834	1.1947E-14
5	0.846217384	1.54832E-13

Table 9. *Levene test for quality of variance for relative intensity*

Levene Statistic	Levene p-value
55.1701579	4.216E-74

Table 10. *Kruskal-Wallis test for relative intensity*

Kruskal-Wallis Statistic	Kruskal-Wallis p-value
271.1755723	8.55007E-55

Table 11. *Dunn's post-hoc pairwise test for relative intensity comparison*

Group 1	Group 2	p-value
0.05	0.05	0.60543
0.05	0	0.000885
0.05	0.5	6.91E-05
0.05	5	3.4E-17
0.05	5	9.59E-06
0.05	0.5	8.42E-33
0.05	0	1E-21
0.05	0	4.69E-11
0.05	0.5	0.000368
0.05	5	2.76E-18
0.05	5	5.73E-05
0.05	0.5	8.69E-34
0.05	0	8.14E-23
0	0.5	2.49E-07
0	5	9.59E-10
0	5	4.01E-12
0	0.5	4.42E-25
0	0	6.56E-14
0.5	5	6.25E-26
0.5	5	0.561864
0.5	0.5	8.96E-40
0.5	0	3.84E-30
5	5	6.4E-27
5	0.5	0.009042
5	0	0.05941
5	0.5	2.06E-40
5	0	4.81E-31
0.5	0	2.31E-05

A2 Mean neurite length statistics

Table 12. *Color and number legend for statistics*

Color legend	Rapamycin conc. [µM]
non-EMF	0
EMF	0.05
	0.5
	5

Table 13. *Descriptive statistics for mean neurite length*

Group	Mean	Standard Error	N
0	64.41513824	7.38410495	67
0	48.38884606	2.817198789	432
0.05	58.37347358	2.846788605	140
0.05	55.21725778	3.263710575	49
0.5	94.1155279	5.926265561	95
0.5	132.7534441	8.412847283	82
5	60.80923863	4.26746729	162
5	77.78152255	5.767224683	192

Table 14. *Shapiro-Wilk test for normalcy of data, mean neurite length*

Group	Shapiro-Wilk Statistic	Shapiro-Wilk p-value
0	0.525924117	2.83474E-13
0	0.882870586	4.21759E-07
0.05	0.730811604	8.15215E-26
0.05	0.916327177	5.22461E-05
0.5	0.762096049	9.8191E-14
0.5	0.832515222	2.42037E-12
5	0.908398101	0.00118727
5	0.610986648	1.1979E-20

Table 15. *Levene test for quality of variance for mean neurite length*

Levene Statistic	Levene p-value
13.11308613	2.3411E-16

Table 16. *Kruskal-Wallis test for mean neurite length*

Kruskal-Wallis Statistic	Kruskal-Wallis p-value
178.7718535	3.53966E-35

Table 17. *Dunn's post-hoc pairwise test for mean neurite length comparison*

Group 1	Group 2	p-value
0.05	0.05	0.122744
0.05	0	0.021394
0.05	0.5	1.77E-30
0.05	5	0.014926
0.05	5	5.93E-07
0.05	0.5	1.26E-16
0.05	0	0.947143
0.05	0	0.474753
0.05	0.5	1.27E-10
0.05	5	0.310148
0.05	5	0.060832
0.05	0.5	8.08E-06
0.05	0	0.199348
0	0.5	2.49E-07
0	5	0.726917
0	5	0.365523
0	0.5	0.000761
0	0	0.051787
0.5	5	2.9E-05
0.5	5	4.88E-09
0.5	0.5	0.030559
0.5	0	1.7E-16
5	5	0.696842
5	0.5	0.009042
5	0	0.032842
5	0.5	0.00078
5	0	0.000442
0.5	0	9.25E-10

A3 Mean SGN soma radius statistics

Table 18. *Color legend for statistics*

Color legend	Rapamycin conc. [μM]
non-EMF	0
EMF	0.05
	0.5
	5

Table 19. *Descriptive statistics for mean SGN soma radii*

Group	Mean	Standard Error	N
0	4.095143644	0.146947416	131
0	3.652838819	0.096689379	277
0.05	4.117735515	0.086532648	55
0.05	5.545542977	0.175949602	47
0.5	3.89977351	0.112048954	63
0.5	4.807905611	0.159450014	56
5	4.528658883	0.159810158	151
5	3.252963658	0.226810174	63

Table 20. *Shapiro-Wilk test for normalcy of data for mean SGN soma radii*

Group	Shapiro-Wilk Statistic	Shapiro-Wilk p-value
0	0.454596072	6.30296E-20
0	0.854410724	2.60622E-06
0.05	0.758032727	7.49702E-20
0.05	0.889651059	9.65964E-05
0.5	0.454596072	6.30296E-20
0.5	0.800429724	4.48608E-13
5	0.8661297	8.3038E-05
5	0.255708469	8.09207E-23

Table 21. *Levene test for quality of variance for mean SGN soma radii*

Levene Statistic	Levene p-value
2.786995145	0.00714828

Table 22. *Kruskal-Wallis test for mean SGN soma radii*

Kruskal-Wallis Statistic	Kruskal-Wallis p-value
183.2603457	3.98953E-36

Table 23. *Dunn's post-hoc pairwise test for mean SGN soma radii comparison*

Group 1	Group 2	p-value
0.05	0.05	1.04E-10
0.05	0	0.726031
0.05	0.5	0.001758
0.05	5	0.012086
0.05	5	3.93E-17
0.05	0.5	0.213572
0.05	0	0.045591
0.05	0	2.41E-06
0.05	0.5	5.62E-05
0.05	5	0.00596
0.05	5	9.99E-31
0.05	0.5	1.46E-11
0.05	0	2.46E-11
0	0.5	0.09257
0	5	0.081622
0	5	3.94E-09
0	0.5	0.252534
0	0	0.07297
0.5	5	0.622027
0.5	5	4.14E-24
0.5	0.5	0.000175
0.5	0	7.12E-05
5	5	4.44E-14
5	0.5	0.001929
5	0	0.000465
5	0.5	7.74E-10
5	0	6E-05
0.5	0	0.338824

A4 Proportion of developed SGNs in culture

Table 24. *Color legend and rapamycin concentrations*

Color legend	Rapamycin conc. [μM]
non-EMF	0
EMF	0.05
	0.5
	5

Table 25. *Statistics for comparison of proportions of developed SGNs in culture, Z-test*

Group 1	Group 2	Proportion 1	Proportion 2	SE1	SE2	Z-statistic	P-value
0.05	0	0.557734205	0.285714286	0.023182	0.025175	7.52882	5.12E-14
0.05	5	0.557734205	0.094252874	0.023182	0.014009	14.70573	5.92E-49
0.05	0.5	0.557734205	0.092057762	0.023182	0.012283	16.05383	5.37E-58
0.05	0.05	0.557734205	0.181102362	0.023182	0.024164	9.746768	1.9E-22
0.05	0.5	0.557734205	0.509868421	0.023182	0.028671	1.298489	0.194119
0.05	5	0.557734205	0.483091787	0.023182	0.034733	1.787345	0.073882
0.05	0	0.557734205	0.126361656	0.023182	0.015508	13.77537	3.59E-43
0	5	0.285714286	0.094252874	0.025175	0.014009	6.843585	7.72E-12
0	0.5	0.285714286	0.092057762	0.025175	0.012283	7.477338	7.58E-14
0	0.05	0.285714286	0.181102362	0.025175	0.024164	2.920523	0.003494
0	0.5	0.285714286	0.509868421	0.025175	0.028671	-5.73496	9.75E-09
0	5	0.285714286	0.483091787	0.025175	0.034733	-4.60758	4.07E-06
0	0	0.285714286	0.126361656	0.025175	0.015508	5.564917	2.62E-08
5	0.5	0.094252874	0.092057762	0.014009	0.012283	0.117968	0.906093
5	5	0.094252874	0.181102362	0.014009	0.024164	-3.31116	0.000929
5	0.5	0.094252874	0.509868421	0.014009	0.028671	-12.5941	2.28E-36
5	5	0.094252874	0.483091787	0.014009	0.034733	-11.1234	9.65E-29
5	0	0.094252874	0.126361656	0.014009	0.015508	-1.52912	0.126234
0.5	0.05	0.092057762	0.181102362	0.012283	0.024164	-3.61547	0.0003
0.5	0.5	0.092057762	0.509868421	0.012283	0.028671	-13.7043	9.57E-43
0.5	5	0.092057762	0.483091787	0.012283	0.034733	-12.0363	2.29E-33
0.5	0	0.092057762	0.126361656	0.012283	0.015508	-1.75393	0.079443
0.05	0.5	0.181102362	0.509868421	0.024164	0.028671	-8.05611	7.88E-16
0.05	5	0.181102362	0.483091787	0.024164	0.034733	-6.93286	4.12E-12
0.05	0	0.181102362	0.126361656	0.024164	0.015508	1.983139	0.047352
0.5	5	0.509868421	0.483091787	0.028671	0.034733	0.59429	0.552318
0.5	0	0.509868421	0.126361656	0.028671	0.015508	11.56132	6.47E-31
5	0	0.483091787	0.126361656	0.034733	0.015508	10.01632	1.29E-23

B Appendix: Raw count of SGNs for each image used for the proportion analysis

Table 26. *Color legend and rapamycin concentrations*

Color legend	Rapamycin conc. [µM]
non-EMF	0
EMF	0.05
	0.5
	5

Table 27. *Table of all data collected for the developed to undeveloped proportions analysis*

Image	Group	Developed count	Global count
1	0	12	23
2	0	23	55
3	0	49	95
4	0	5	30
5	0	3	119
6	0.05	40	108
7	0.05	51	108
8	0.05	45	90
9	0.05	66	77
10	0.05	54	76
11	0.5	7	93
12	0.5	7	63
13	0.5	13	61
14	0.5	6	57
15	0.5	8	100
16	0.5	3	60
17	0.5	3	24
18	0.5	4	96
19	5	18	126
20	5	4	46
21	5	3	55
22	5	11	145
23	5	5	63
24	0	9	147
25	0	7	65

26	0	22	149
27	0	6	53
28	0	14	45
29	0.05	6	16
30	0.05	21	25
31	0.05	34	44
32	0.05	17	38
33	0.05	36	116
34	0.05	41	65
35	0.5	3	4
36	0.5	3	6
37	0.5	26	39
38	0.5	16	57
39	0.5	52	101
40	5	2	4
41	5	2	35
42	5	9	31
43	5	12	37
44	5	5	48
45	5	10	47
46	5	6	52